**ORIGINAL PAPER**

# Extracellular matrix stiffness controls VEGF$_{165}$ secretion and neuroblastoma angiogenesis via the YAP/RUNX2/SRSF1 axis

Min Bao[1] · Yi Chen[1] · Ji-Ting Liu[1] · Han Bao[1] · Wen-Bin Wang[1] · Ying-Xin Qi[1] · Fan Lv[2]

## Abstract

Aberrant variations in angiogenesis have been observed in tumor tissues with abnormal stiffness of extracellular matrix (ECM). However, it remains largely unclear how ECM stiffness influences tumor angiogenesis. Numerous studies have reported that vascular endothelial growth factor-A (VEGF-A) released from tumor cells plays crucial roles in angiogenesis. Hence, we demonstrated the role of ECM stiffness in VEGF-A release from neuroblastoma (NB) cells and the underlying mechanisms. Based on 17 NB clinical samples, a negative correlation was observed between the length of blood vessels and stiffness of NB tissues. In vitro, an ECM stiffness of 30 kPa repressed the secretion of VEGF$_{165}$ from NB cells which subsequently inhibited the tube formation of human umbilical vein endothelial cells (HUVECs). Knocked down VEGF$_{165}$ in NB cells or blocked VEGF$_{165}$ with neutralizing antibodies both repressed the tube formation of HUVECs. Specifically, 30 kPa ECM stiffness repressed the expression and nuclear accumulation of Yes-associated protein (YAP) to regulate the expression of Serine/Arginine Splicing Factor 1 (SRSF1) via Runt-related transcription factor 2 (RUNX2), which may then subsequently induce the expression and secretion of VEGF$_{165}$ in NB tumor cells. Through implantation of 3D col-Tgels with different stiffness into nude mice, the inhibitory effect of 30 kPa on NB angiogenesis was confirmed in vivo. Furthermore, we found that the inhibitory effect of 30 kPa stiffness on NB angiogenesis was reversed by YAP overexpression, suggesting the important role of YAP in NB angiogenesis regulated by ECM stiffness. Overall, our work not only showed a regulatory effect of ECM stiffness on NB angiogenesis, but also revealed a new signaling axis, YAP-RUNX2-SRSF1, that mediates angiogenesis by regulating the expression and secretion of VEGF$_{165}$ from NB cells. ECM stiffness and the potential molecules revealed in the present study may be new therapeutic targets for NB angiogenesis.

**Keywords** Extracellular matrix stiffness · Angiogenesis · Neuroblastoma · Intercellular communication · Mechanobiology

## Introduction

Neuroblastoma (NB) is one of the most common solid malignancy in children that arises from the neural crest. Despite the most advanced multidisciplinary treatments, more than 15% of pediatric cancer patients die of NB [1]. Deep insights into the mechanism of NB pathogenesis are imperative for developing more effective therapeutics. Analysis of The Cancer Genome Atlas (TCGA) showed that the original sites of NB are distributed throughout the body (Supplemental Table S1). The stiffness of the predisposing original sites, such as the predisposing adrenal gland, retroperitoneum, and peritoneum, is less than 10 kPa, while a limited number of NBs originate from stiffer tissues such as bones, joints and articular cartilage, the stiffness of which ranges from 30 kPa to 2 GPa [2]. Accumulating studies have shown that stiffness contributes to the proliferation and metastasis of solid tumors, but the role of tumor stiffness in the malignancy and prognosis of NB is still unclear.

Studies have revealed that changes in solid tumor stiffness are mainly caused by extracellular matrix (ECM) remodeling [3]. The ECM is a complex network of proteins,

✉ Ying-Xin Qi
qiyx@sjtu.edu.cn

✉ Fan Lv
lvfan@xinhuamed.com.cn

1 Institute of Mechanobiology & Medical Engineering, School of Life Sciences & Biotechnology, Shanghai Jiao Tong University, 800 Dongchuan Road, Minhang, 200240 Shanghai, China

2 Department of Pediatric Surgery, Xinhua Hospital, Shanghai Jiao Tong University School of Medicine, 1665 Kongjiang Road, Yangpu, Shanghai 200092, China

proteoglycans and glycoproteins that forms the cell microenvironment. Early studies of ECM stiffness focused on the differentiation of stem cells by seeding cells adherent to polyacrylamide (PAA) gels with variable stiffnesses. Engler et al. found that soft polyacrylamide gels (0.1–1 kPa) promote mesenchymal stem cell (MSC) differentiation toward neurogenesis, intermediate stiffness gels (~ 10 kPa) promote myogenesis, and stiff gels (~ 30 kPa) promote osteogenesis [4]. Recently, an increasing number of studies have focused on the effects of ECM stiffness on tumor pathogenesis. During tumor progression, an imbalance in ECM stiffness has a profound impact on tumor growth [5]. Studies based on xenografts in nude mice have shown that compared with a soft ECM (0.4 kPa), a stiff ECM (9 kPa) promotes tumor formation by MCF7 breast cancer cells [6]. Furthermore, lung cancer cells [7], glioma cells [8], and breast cancer cells [9] exhibit higher level of cell viability-related activities, including proliferation and migration, when seeded on stiffer PAA gels (5.7–120 kPa) compared with softer gels (0.15–0.5 kPa). However, the NB tumor cell line SK-N-DZ showed repression of proliferation as the stiffness of the PAA gels increased from 1 to 300 kPa [10].

Multiple studies have demonstrated the important role of ECM stiffness in regulating tumor angiogenesis. Francois et al. showed that reducing the stiffness of the breast cancer tumors reduces the extent of angiogenesis within the tumor in vivo [11]. Furthermore, ECM from colon tumor is stiffer than normal human colon tissue and promotes vascular network formation during tumor growth in vivo [12]. In liver cancer, inhibiting ECM deposition, which decreased ECM stiffness, increased the antiangiogenic effects of the antitumor drug bevacizumab [13].

It is well established that tumor angiogenesis requires communication between tumor cells and endothelial cells (ECs). Studies have shown that coculture of melanoma cells and ECs promotes the recruitment of mature ECs and the formation of capillary-like structures in vitro [14]. Prior studies have demonstrated that osteosarcoma cells secret VEGF-A, a proangiogenic factor, to promote tube formation of ECs, which may participate in angiogenesis [15]. In NB, VEGF-A is also the most common pro-angiogenic factor and its expression correlated with disease stage [16]. Evidence has shown that inhibiting PI3K/mTOR activation could suppress the paracrine release of VEGF-A from NB cells and reduce the angiogenic capacity of ECs [17]. Many clinical studies have used anti-VEGF-A agents, such as bevacizumab to inhibit tumor angiogenesis including NB [18]. VEGF-A has different isoforms that are regulated by alternative splicing. The major isoforms are $VEGF_{165}$, $VEGF_{189}$ and $VEGF_{121}$, among which $VEGF_{165}$ is the most potent initiator of angiogenesis [19]. However, whether ECM stiffness influences the paracrine release of $VEGF_{165}$ from tumor cells and the tube formation capacity of ECs are largely unknown.

In the present study, we hypothesized that ECM stiffness regulates NB angiogenesis by modulating the intercellular communication between NB tumor cells and ECs. Analysis of clinical NB samples showed a potential correlation between ECM stiffness and angiogenesis. In addition, in vitro studies demonstrated the roles of ECM stiffness in $VEGF_{165}$ secretion from NB tumor cells and the subsequent effect on EC tube formation capacity. A 3D culture system in nude mice, which more accurately recapitulates the native environment, was further adopted to better understand the effects of ECM stiffness on NB angiogenesis. Our research revealed the regulatory mechanism of ECM stiffness on NB angiogenesis and may provide potential targets for the evaluation of NB malignancies and also for their clinical therapy.

## Methods

### Human NB samples

Human clinical NB samples were obtained from patients in Shanghai Xinhua Hospital. All samples were obtained with the agreement of the patients and approval from the Medical Ethics Committee of Xinhua Hospital Affiliated with Shanghai Jiao Tong University School of Medicine. The study was strictly carried out in accordance with the Declaration of Helsinki and International Ethical Guidelines for Health-related Research Involving Humans. Hematoxylin & Eosin (H&E) staining, immunofluorescence staining, and stiffness measurements were carried out on the human samples in accordance with the approved guidelines. The basic information of all 17 NB patients was provided in Supplemental Table S2.

### Measurement of the stiffness of NB clinical sample tissues

The stiffness of NB clinical sample tissues were measured by Piuma Nanoindenter (Optics11). As previously described [20], fiber-optical Fabry-Perot interferometry combined with a monolithical cantilever-based probe was used to examine local micro-elasticity with high accuracy and precision. We used the probe with a 0.18 N/m spring constant and a 9 μm spherical indentation tip. We fixed the sample tissues onto the bottom of a Petri dish and then submerged them in buffer at room temperature with the nanoindenter tip remaining well below the surface of buffer at all times. The indents were depth controlled (10 μm) and the loading and unloading period was set to be 2 s. The stiffness was calculated using the Hertz spherical indentation model.

## 3D Col-Tgel culture and tumor induction in nude mice

Nude mice were purchased from Vital River Laboratory Animal Technology Company. The animal care and experimental protocols were performed in accordance with the Animal Management Rules of China (55, 2001, Ministry of Health, China), and the study was approved by the Animal Research Committee of Shanghai Jiao Tong University.

SK-N-SH cells were trypsinized with 0.125% trypsin and then $1 \times 10^6$ cells were mixed with 100 μL Col-Tgels of different stiffness which were prepared according to manufacturer's instructions (Hong Rong Micro Re, P1720). Then Col-Tgels with SK-N-SH cells were injected into subcutaneous abdomen of 5-week-old male nude mice after anesthetizing with isoflurane. Col-Tgels were excised after 7 days.

## H&E staining and immunofluorescence staining

For H&E and immunofluorescence staining, tissue slides were fixed in 4% paraformaldehyde, dehydrated in 30% sucrose solution, and then cut into 6-μm sections. H&E staining were performed as manufacturer's instructions (Beyotime, C0105S).

For immunofluorescence staining, cells and tissue slides were fixed in 4% paraformaldehyde. Tissue slides were performed for antigen retrieval with citrate buffer (pH 6.0) at 95 °C for 15 min. Slides were blocked with 10% goat serum for 1 h and then immunostained with specific antibodies against YAP (1:100, Cell Signaling Technology), SRSF1 (1:100, Proteintech), CD31(1:100, Thermo Fisher), CD105 (1:100, Abcam), von Willebrand factor (vWF) (1:200, Proteintech) at 4 °C overnight. After washing in PBS, the samples were incubated with fluorochrome-conjugated secondary antibodies in blocking buffer. Nucleus was stained with DAPI. Finally, images were captured using a laser-scanning confocal microscopy (Olympus IX81). Three random fields in each tissue slice were selected and the average immunofluorescence intensity was calculated. For each field, the immunofluorescence intensity is mean immunofluorescence intensity (Integrated Density/Area) which was analyzed with ImageJ software.

## Cell culture

SK-N-SH, the NB cell line, was purchased from Chinese Academy of Sciences Shanghai Cell Bank (Shanghai, China), and cultured in DMEM medium with the addition of 10% FBS and 0.5% penicillin-streptomycin, at 37 °C and 5% $CO_2$. HUVECs were harvested by collagenase treatment from umbilical cord veins [21] and cultured in endothelial cell basal medium-2 (Lonza).

## Substrate preparation

Polyacrylamide gels with variable stiffness were prepared according to a previously established protocol [22]. Briefly, acrylamide and bis-acrylamide mixture with indicated concentrations was allowed to polymerize on a glass slide, and the gel was then covered with sulfosuccinimidyl-6-[4′-azido-2′-nitrophenylamino] hexanoate (Sulfo-SANPAH; Pierce). After exposure to UV light for 10 min twice, the polyacrylamide sheet was washed twice and incubated with a solution of 0.1% gelatin overnight at 4 °C. The stiffness of gels in our researches were 1 kPa, 8 kPa and 30 kPa, respectively.

## Tube formation assay

The conditioned medium from SK-N-SH cells cultured on 1 kPa, 8 kPa, 30 kPa and plastic substrates were, respectively, used to pretreat HUVECs for 24 h in 6-well plates. Matrigel (BD Biosciences, Bedford, MA) was thawed at 4 °C overnight, added to 24-well plates with 400 μL per well, and incubated at 37 °C, 5% $CO_2$ for 30 min. The pretreated HUVECs were trypsinized with 0.125% trypsin and then terminated trypsinization with endothelial cell basal media-2 (Lonza). After that, $1 \times 10^4$ cells were plated onto the Matrigel in endothelial cell basal medium-2 (Lonza). After incubation at 37 °C with 5% $CO_2$ for 6 h, the vascular network of HUVECs was visualized by microscopy (Olympus, DP72). The total tube length, number of junctions and tube percentage area were measured using imaging analysis software (Angiotool).

## Western blot and antibodies

SK-N-SH cells were gently washed with cold PBS and lysed at 4 °C for 5 min with lysis buffer (0.15 M Tris, pH 6.8; 1.2% SDS; 15% mercaptoethanol). Lysates were subjected to electrophoretic separation by 10% SDS-PAGE and transferred to a PVDF membrane. The membrane was blocked for 1 h in 5% non-fat milk and incubated with primary antibodies: YAP (1:500; Cell Signaling Technology), phosphorylated YAP (S127) (1:500; Cell Signaling Technology), TAZ (1:500; Cell Signaling Technology), phosphorylated TAZ (1:500; Cell Signaling Technology), SRSF1 (1:1000; Proteintech), RUNX2 (1:1000, Cell Signaling Technology), LaminA/C (1:1000; Santa Cruz Biotechnology), PCNA (1:1000; Proteintech) and GAPDH (1:1000; Proteintech). The membranes were then incubated with horseradish peroxidase-conjugated anti-mouse or anti-rabbit IgG (1:1000; Cell Signaling Technology), and were developed using enhanced chemiluminescence (ECL; Tanon, Shanghai, China). The

chemiluminescent signals were captured with the Odyssey Fc Imaging System (LI-COR Biosciences, Lincoln, NA), and then quantified with Quantity One software (Bio-Rad, Hercules, CA). The nuclear and cytoplasmic proteins were separated with Nuclear and Cytoplasmic Protein Extraction Kit. The procedure was operated according to manufacturer's instructions (Beyotime, P0027).

## Quantitative real-time polymerase chain reaction (qRT-PCR)

RNA was extracted from cell samples with Trizol Reagent (Invitrogen) and the obtained total RNA was reversely transcribed using oligo dT (Thermo Fisher Scientifc). qRT-PCR was performed using SYBR Green Supermix (TaKaRa) and analyzed with the StepOne Real-Time PCR System (Applied Biosystems). Fold change of mRNA was calculated using a $2^{-\Delta\Delta CT}$ method. All specific primer sequences are shown in Supplemental Table S3.

## Enzyme-linked immunosorbent assay (ELISA) assay

The $VEGF_{165}$ concentrations in the conditioned medium from SK-N-SH cells were detected using human $VEGF_{165}$ ELISA Kit (Xinfan Bio-Technology, XF-Human-1817) following manufacturer's protocol. Briefly, 50 μL of standard or diluent samples (dilution ratio = 5) were pipetted to wells that were layered with capture antibody. 100 μL of detection antibody was added to each well and incubated for 60 min at 37 °C. After 4 washing cycles, 50 μl chromogen solution A and 50 μl chromogen solution B were added to each well. Wells were gently mixed and incubated for 15 min at 37 °C, then 50 μL stop solution was added. OD450 nm was employed using a plate reader (Bio-Rad 680).

## Transfection with small interfering RNA

For the RNA interference (RNAi) experiment, SK-N-SH cells were transfected with small interfering RNA (siRNA) or scrambled siRNA (Shanghai Gene-Pharma) at a concentration of 100 nM with 5 μL Lipofectamine™ 2000 (Invitrogen) in Opti-MEM (Gibco) for 48 h according to the manufacturer's instructions. The medium was supplied with 1 mL cells cultured medium after 8 h post-transfection. The sequences of the siRNA oligos, are listed in Supplemental Table S4.

## Construction and transfection of YAP overexpression plasmid

The complete coding sequences (CDS) of YAP (NM_006106.5) was obtained by gene amplification with designed primer (Sangon Biotech) which is listed in Supplemental Table S3. A green fluorescent protein (GFP, 26.9 kDa) was added behind the coding sequence of YAP to track and ensure the transfection. Then the fragments were subcloned into the pcDNA-3.3 vector with restriction sites XhoI and BamHI (Thermo Fisher). Plasmid constructs were verified by DNA sequencing (Sangon Biotech). The normal function of YAP with YAP-GFP overexpression construct has been demonstrated by previous researches [23]. YAP-overexpressing plasmid or empty pcDNA-3.3 vector were transfected into SK-N-SH cells using Lipofectamine™ 2000 (Invitrogen) DNA Transfection Reagent according to the manufacturer's protocol. Transfection efficiency was confirmed by Western blot.

## Chromatin immunoprecipitation

Chromatin immunoprecipitation (ChIP) assay was performed with Chromatin Immunoprecipitation Kit following manufacturer's instructions (BersinBio™, Catalog Bes5001). Antibodies used for immunoprecipitation were rabbit anti-RUNX2 (Cell Signaling Technology) and rabbit IgG (BersinBio™). Immunoprecipitated DNA was analyzed by qRT-PCR using SYBR Green Supermix (TaKaRa) and StepOne Real-Time PCR System (Applied Biosystems). Fold change of mRNA was analyzed using a $2^{-\Delta\Delta CT}$ method. Primers for qRT-PCR are listed in Supplemental Table S3.

## Statistical analysis

All experiments were performed at least three separate times. The mean values of the qPCR, and Western blotting data (except the ChIP data) were first quantified to GAPDH, and then normalized to plastic groups. Statistical analysis was performed with the Graphpad Prism 7 program using one-way ANOVA to compare differences among the four groups, and Student's $t$-test to compare differences between two groups. $P < 0.05$ was considered statistically significant (*) and $P < 0.01$ was considered highly significant (**).

## Results

### Tissue stiffness of NB clinical samples

The original sites of 17 clinical NB samples were from retroperitoneum (15 samples including 13 adrenal area and 2 pelvic cavity) and posterior superior mediastinum (2 samples) (Supplemental Table S2), which were consistent with the distributional trend analyzed with The Cancer Genome Atlas (TCGA) (Supplemental Table S1). The stiffness of samples was measured with a Piuma Nanoindenter. The mean stiffness values of these clinical samples ranged from 0.174 to 8.452 kPa (Fig. 1A). To evaluate the
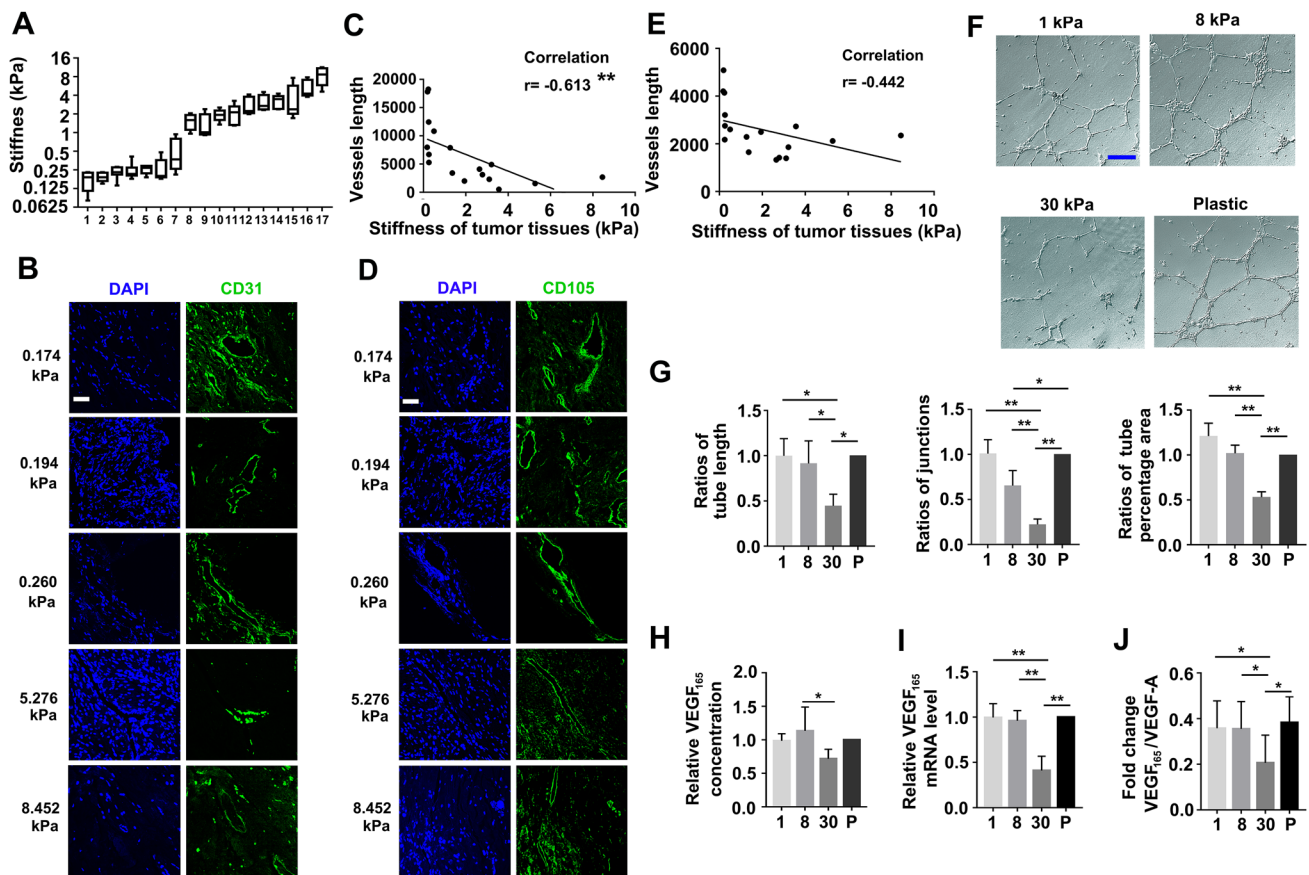
**Fig. 1** Angiogenesis is negatively related to stiffness in NB clinical samples and *in vitro* culture system. **A** Stiffness of 17 human NB clinical samples was measured by nanoindentation. Each sample was measured at least five times in different regions. **B** Immunostaining of CD31 (green) in representative NB samples (scale bar $=40$ μm). **C** The correlation between vessels length and tissues stiffness of human NB samples. Angiogenic vessels in human NB samples were immunostained by CD31, and the length was measured by Angiotool software. **D** Immunostaining of CD105 (green) in representative NB samples (scale bar $=40$ μm). **E** The correlation between vessels length and tissues stiffness of human NB samples. Angiogenic ves-

sels in human NB samples were immunostained by CD105, and the length was measured by Angiotool software. **F** The tube formation of HUVECs stimulated by conditioned medium from SK-N-SH cells cultured on different stiffness substrates (scale bar $=100$ μm) ($n=3$). **G** The total tube length, number of junctions and tube percentage area were measured by Angiotool software. **H** Secretion levels of $VEGF_{165}$ from SK-N-SH cells ($n=5$). **I** The mRNA level of $VEGF_{165}$ normalized to GAPDH in SK-N-SH cells ($n=313$). **J** The mRNA level of $VEGF_{165}$ as a proportion of the total VEGF-A ($n=10$). Values were shown as the mean $\pm$ SD, $*P < 0.05$, $**P < 0.01$ vs. the indicated groups

angiogenic capability of samples with different stiffnesses, staining for CD31, CD105 and vWF, the markers of ECs, was performed (Fig. 1B and D, Supplemental Fig. 1A). In softer NB samples (0.174 kPa, 0.194 kPa and 0.260 kPa), a large number of blood vessels were observed. However, fewer blood vessels were detected in stiffer NB samples (5.276 kPa, 8.452 kPa). Then, the relationship between the angiogenic capability and the stiffness in all 17 NB clinical samples was evaluated, and linear regression revealed a negative association ($r = -0.613$ for CD31, $r = -0.442$ for CD105, $r = -0.557$ for vWF) between blood vessel length and stiffness in NB samples (Fig. 1C and E, Supplemental Fig. 1B). Our in vivo data suggested that NB angiogenesis was associated with ECM stiffness.

## ECM stiffness regulated VEGF-A expression and angiogenesis in vitro

To confirm the relationship between angiogenesis and stiffness in NB, in vitro studies with substrates of different stiffnesses (1 kPa, 8 kPa and 30 kPa, which covered the major stiffness range of human tissues), were performed. A plastic surface with a stiffness in the gigapascal (GPa) range was used for the control group [24]. To investigate whether NB responded to ECM stiffness and modulates angiogenesis via VEGF-A secretion, conditioned medium from the NB cell line SK-N-SH cultured on substrates of different stiffnesses were used to stimulate HUVECs to form capillary structures.

Through microscopic observation, we found that compared with the medium from SK-N-SH cells cultured on the 1 kPa, 8 kPa and plastic substrates, conditioned medium from SK-N-SH cells cultured on the 30 kPa substrate significantly inhibited tube formation of HUVECs (Fig. 1F). Three important features of the vascular networks, i.e., the total tube length, number of junctions and tube percentage area, were quantified using AngioTool software (NCI). The results revealed that all three of these parameters were significantly decreased in HUVECs stimulated by conditioned medium SK-N-SH cells cultured on the 30 kPa substrate in comparison with those from SK-N-SH cells cultured on the 1 kPa, 8 kPa and plastic substrates (Fig. 1G).

$VEGF_{165}$ can be secreted by different kinds of tumor cells and plays an important role during tumor angiogenesis [25]. Hence, we evaluated the secretion of $VEGF_{165}$ from SK-N-SH cells cultured on substrates with different stiffnesses with ELISA. The secretion of $VEGF_{165}$ was significantly decreased at 30 kPa when compared with 8 kPa, and showed a decreasing trend when compared with that on the 1 kPa and plastic substrates. (Fig. 1H). Furthermore, the mRNA expression level of $VEGF_{165}$(Fig. 1I) and the ratio of $VEGF_{165}$ relative to total VEGF-A (Fig. 1J) were both significantly decreased in the 30 kPa group compared with the 1 kPa and 8 kPa and plastic groups.

Furthermore, the direct evidence for $VEGF_{165}$ on tube formation was detected with exogenetic $VEGF_{165}$ stimulation, $VEGF_{165}$ neutralizing antibody and specific siRNA transfection. The results revealed that recombinant human $VEGF_{165}$ significantly increased the tube formation capacity, which was evaluated by total tube length, number of junctions and tube percentage area (Supplemental Fig. 2A, B). $VEGF_{165}$ neutralizing antibody remarkably reversed the effect of $VEGF_{165}$ on tube formation capacity of HUVECs (Supplemental Fig. 2A, 2B). We also knocked down the $VEGF_{165}$ in SK-N-SH cells by si-RNA transfection. The interference efficiency was determined by qPCR analysis (Supplemental Fig. 2 C). $VEGF_{165}$ ELISA showed that $VEGF_{165}$ concentration in the medium after specific siRNA transfection was significantly decreased (Supplemental Fig. 2D). The tube formation capacity of HUVECs pretreated with conditioned medium from $VEGF_{165}$ knocked down group was also significantly decreased (Supplemental Fig. 2E, F).

Collectively, the above in vitro data suggested that a stiffness of 30 kPa may decrease the secretion of $VEGF_{165}$ from NB cells via the alternative splicing, which subsequently repress angiogenesis.

## SRSF1 expression in SK-N-SH cells was responsive to ECM stiffness

Serine/arginine-rich (SR) proteins are essential splicing regulators required for VEGF-A alternative splicing [26].

Bioinformatics analysis with Ingenuity Pathway Analysis (IPA) software revealed that among 12 SR family members, SRSF1, SRSF3, SRSF5 and SRSF6 were predicted to regulate VEGF-A (Fig. 2A). Then, we investigated whether ECM stiffness induces the expression of these four SR members. As shown in Fig. 2B, the mRNA expression of SRSF1 was significantly decreased in the 30 kPa group compared with the 1 kPa and plastic groups. Compared to that at 8 kPa, the mRNA expression of SRSF1 at 30 kPa showed a decreasing trend. The mRNA expression levels of the other three SRSF proteins, i.e., SRSF3, SRSF5 and SRSF6, were similar in cells cultured on the 1 kPa, 8 kPa, 30 kPa and plastic substrates (Fig. 2B). This result suggested that only SRSF1 showed a trend similar to that of $VEGF_{165}$ secretion at different stiffnesses.

Hence, we focused on the potential mechanism by which SRSF1 expression is regulated by ECM stiffness. Immunostaining showed the expression of SRSF1 in NB clinical samples with different stiffnesses (Fig. 2C). In the stiffer sample (8.452 kPa), the expression of SRSF1was decreased compared with that in the softer sample (0.174 kPa) (Fig. 2D). The protein expressions of SRSF1 in all 17 NB patient samples were measured by Western blot (Supplemental Fig. 3A and D), and linear regression revealed a negative association ($r = -0.361$) (Supplemental Fig. 3E). These results indicated that in NB, SRSF1 expression is modulated in response to ECM stiffness.

To further confirm this hypothesis, the protein level and the subcellular distribution of SRSF1 in SK-N-SH cells cultured under different stiffness conditions were detected in vitro. Western blot analysis showed that SRSF1 protein levels were significantly decreased in cells cultured on the 30 kPa substrate compared with those cultured on the 1 kPa, 8 kPa and plastic substrates (Fig. 2E). Immunofluorescence staining also confirmed that SRSF1 only accumulated in the nucleus (Fig. 2F). Nuclear-cytoplasmic separation combined with Western blot analysis showed that SRSF1 was only present in nuclear extracts referenced with the nuclear protein LaminA/C (Fig. 2G). In addition, the immunofluorescence intensity of SRSF1 was significantly decreased in the 30 kPa group compared with the 1 kPa, 8 kPa and plastic groups (Fig. 2H).

Furthermore, whether the changed expression of SRSF1 can regulate angiogenesis by modulating the expression of $VEGF_{165}$ was investigated. After siRNA transfection to knock down SRSF1 in SK-N-SH cells, the interference efficiency was determined by Western blot analysis (Supplemental Fig. 4 A). The mRNA expression of $VEGF_{165}$ showed a significant decrease after SRSF1 interference (Fig. 2I). $VEGF_{165}$ secretion was also obviously reduced when SRSF1 was attenuated by siRNA (Fig. 2J). Conditioned medium from SK-N-SH cells transfected with SRSF1 siRNA markedly decreased the total tube length and number
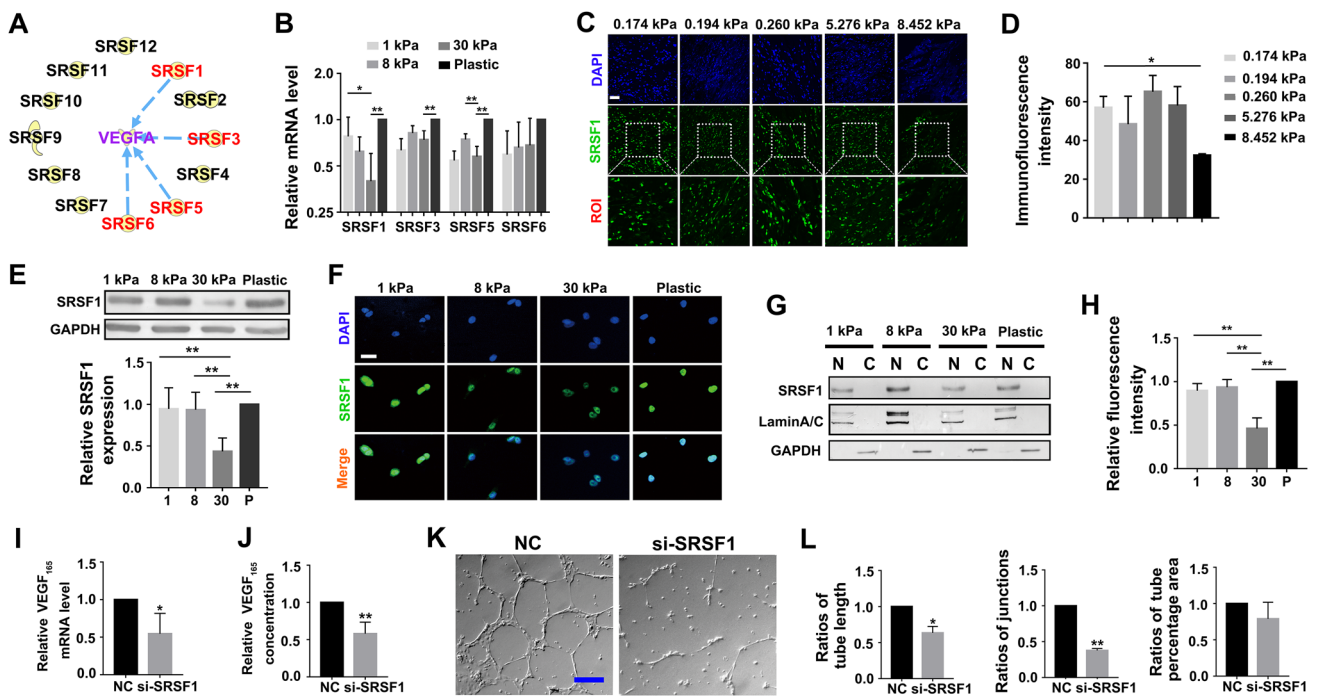
**Fig. 2** Nuclear SRSF1 expression is regulated by ECM stiffness which modulates NB angiogenesis *in vitro*. **A** The potential regulators in SR family to VEGF-A were predicted with IPA software (Qiagen, https://www.qiagenbioinformatics.com/products/ingenuitypathway-analysis, content version: 57,662,101/). **B** The mRNA levels of SRSF1, SRSF3, SRSF5 and SRSF6 in SK-N-SH cells on 1 kPa, 8 kPa, 30 kPa and plastic substrates ($n=5$). **C** Immunostaining of SRSF1 (green) in representative NB clinical samples showed SRSF1 expression and subcellular localization (scale bar $=40$ μm). **D** Immunofluorescence intensity of SRSF1 in representative NB clinical samples was measured by ImageJ software. **E** SRSF1 protein levels in SK-N-SH cells on 1 kPa, 8 kPa, 30 kPa and plastic substrates ($n=5$). **F** SRSF1 expression and subcellular localization in SK-N-SH cells measured by immunostaining (scale bar $=10$ μm). **G** Subcellular localization of SRSF1 in SK-N-SH cells measured by Nuclear and Cytoplasmic Protein Extraction Kit ($n=5$). **H** Relative immunofluorescence intensity of SRSF1 in SK-N-SH cells seeded on 1 kPa, 8 kPa, 30 kPa and plastic substrates ($n=3$). **I** The mRNA levels of VEGF$_{165}$ after decreasing SRSF1 by si-RNA in SK-N-SH cells ($n=5$). **(J)** VEGF$_{165}$ secretion levels from SK-N-SH cells after decreasing SRSF1 by si-RNA ($n=5$). **K** The tube formation of HUVECs stimulated by conditioned medium from SK-N-SH cells after decreasing SRSF1 by si-RNA (scale bar $=100$ μm) ($n=3$). **L** The total tube length, number of junctions and tube percentage area were measured by Angiotool software. Values were shown as the mean $\pm$ SD, *$P<0.05$, **$P<0.01$ vs. the indicated groups or negative control (NC)

of junctions of HUVECs compared with that in the negative control group, and the tube percentage area showed a similar tendency (Fig. 2K and L).

The above results showed that ECM stiffness regulates the nuclear expression of SRSF1. Subsequently, SRSF1 modulates the secretion of VEGF$_{165}$ from SK-N-SH cells and further influences the tube formation capacity of HUVECs.

## ECM stiffness modulated the expression and subcellular distribution of YAP

We extended our investigation to the mechanism by which ECM stiffness modulates the expression of SRSF1. Previous studies have revealed that Yes-associated protein (YAP) plays central roles in mechanotransduction [27]. Hence, the expression and subcellular location of YAP were evaluated both in vivo and in vitro.

The immunofluorescence staining results showed that YAP colocalization with DAPI was significantly decreased in the stiffer NB clinical sample (8.452 kPa) compared with the other softer samples, indicating that ECM stiffness might regulate the subcellular localization of YAP (Fig. 3A and B). The protein expressions of YAP in all 17 NB patient samples were also measured by Western blot (Supplemental Fig. 3A and B), and linear regression revealed a negative association ($r = -0.566$) (Supplemental Fig. 3C). These results indicated that YAP expression is in responsive to ECM stiffness in NB.

For in vitro studies, SK-N-SH cells were cultured on substrates with different stiffnesses. Western blot analysis showed that the total expression of YAP was significantly decreased in cells cultured on the 30 kPa compared with 1 kPa, 8 kPa and plastic substrates and that the phosphorylated YAP level also showed an increasing trend at 30 kPa after normalization to the GAPDH level (Fig. 3C).
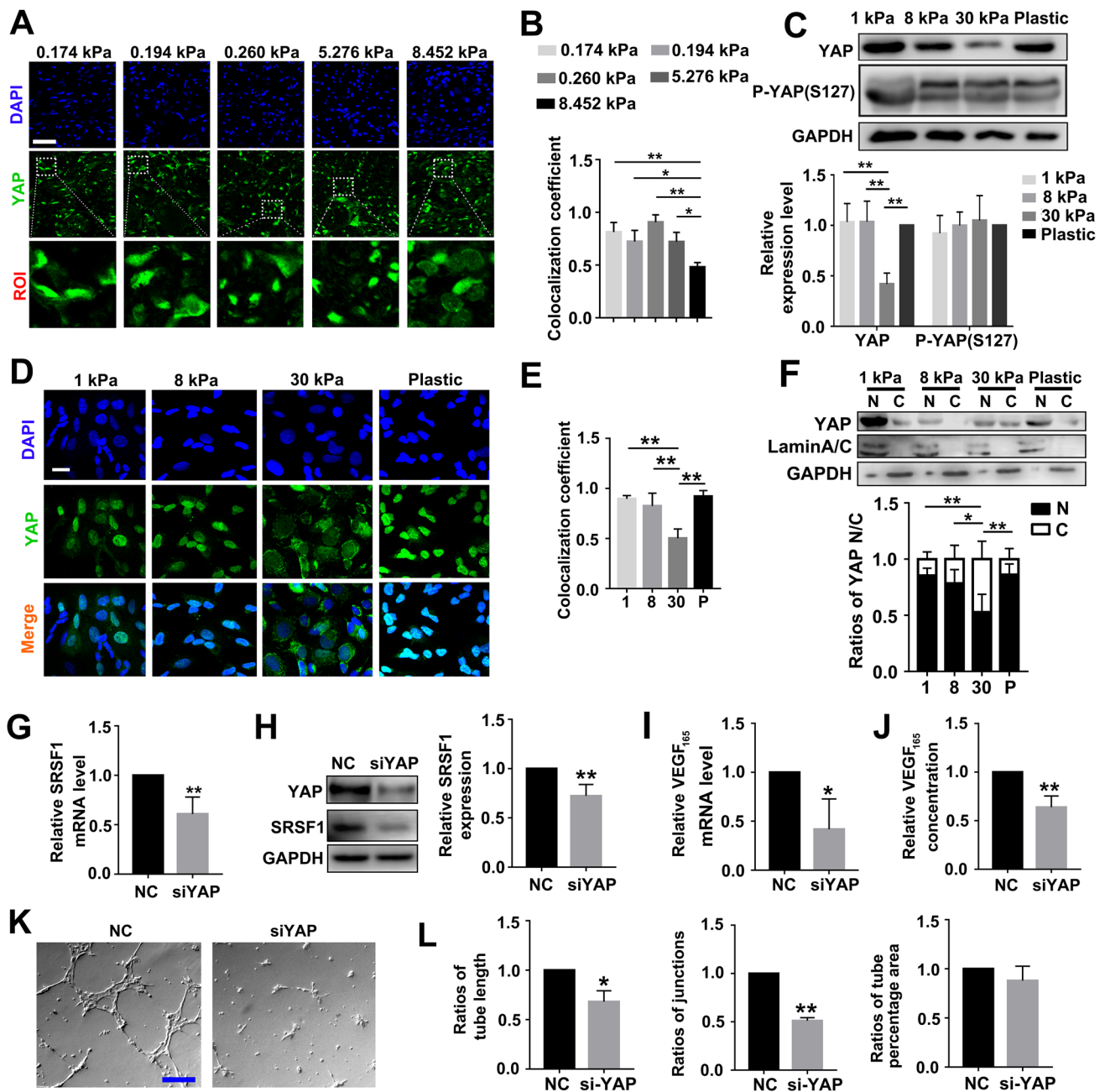
**Fig. 3** ECM stiffness modulates SRSF1, VEGF$_{165}$ secretion and angiogenesis through YAP. **A** Immunostaining of YAP (green) in representative NB clinical samples (scale bar = 40 μm). **B** Colocalization coefficient of YAP with nucleus in representative NB clinical samples was measured by Image Pro software. **C** YAP and phosphorylated YAP(S127) protein levels in SK-N-SH cells seeded on 1 kPa, 8 kPa, 30 kPa and plastic substrates (*n*=5). **D** Immunostaining of YAP (green) in SK-N-SH seeded on 1 kPa, 8 kPa, 30 kPa and plastic substrates (scale bar = 20 μm). **E** Colocalization coefficient of YAP with nucleus in SK-N-SH cells seeded on 1 kPa, 8 kPa, 30 kPa and plastic substrates (*n*=3). **F** Subcellular localization of YAP in SK-N-SH cells measured by Nuclear and Cytoplasmic Protein Extraction Kit

(*n*=5). **G** The mRNA levels of SRSF1 after decreasing YAP by si-RNA in SK-N-SH cells (*n*=5). **H** The protein levels of SRSF1 after decreasing YAP by si-RNA in SK-N-SH cells (*n*=5). **I** The mRNA levels of VEGF$_{165}$ after decreasing YAP by si-RNA in SK-N-SH cells (*n*=5). **J** VEGF$_{165}$ secretion from SK-N-SH cells after decreasing SRSF1 by si-RNA (*n*=5). **K** The tube formation of HUVECs stimulated by conditioned medium from SK-N-SH transfected with YAP specific si-RNA (scale bar = 100 μm) (*n*=3). **L** The total tube length, number of junctions and tube percentage area were measured by Angiotool software. Values were shown as the mean ± SD, *$P<0.05$, **$P<0.01$ vs. the indicated groups or negative control (NC)

Immunostaining of YAP showed that YAP colocalization with DAPI was significantly decreased in SK-N-SH cells cultured on the 30 kPa substrate compared with SK-N-SH cells cultured on the 1 kPa, 8 kPa and plastic substrates (Fig. 3D and E). To further confirm these results, nucleocytoplasmic separation combined with Western blot analysis was performed, and the ratio of YAP expression in the cytoplasm to that in the nucleus was obviously increased on the 30 kPa substrate compared with the 1 kPa, 8 kPa and plastic substrates (Fig. 3F).

We also evaluated the expression and subcellular localization of TAZ (transcriptional coactivator with PDZ-binding motif), which is the paralog of YAP [28], under different stiffness conditions. The results showed that TAZ expression was significantly decreased in cells cultured on the 30 kPa substrate compared with cells cultured on the 1 kPa, 8 kPa and plastic substrates, but there were no obviously differences in the level of phosphorylated TAZ among the different stiffness conditions (Supplemental Fig. 5). In addition, the subcellular localization as detected by Western blot showed that the amount of TAZ in the cytoplasm was significantly increased in the cells cultured on 30 kPa substrate compared with cells cultured on the 1 kPa, 8 kPa and plastic substrates (Supplemental Fig. 6).

These results suggested that in SK-N-SH cells, the 30 kPa stiffness condition not only decreased the expression of YAP and TAZ but also increased their cytoplasmic retention.

## YAP regulated SRSF1 expression, VEGF$_{165}$ secretion and angiogenesis

To investigate the effects of YAP suppression, specific siRNAs were transfected, and the interference efficiency was determined by Western blot analysis (Supplemental Fig. 4B). YAP siRNA significantly decreased the mRNA and protein expression of SRSF1, indicating that YAP regulated SRSF1 expression at the transcriptional level (Fig. 3G and H). In addition, through nucleocytoplasmic separation combined with Western blot and immunostaining of SRSF1, we found that SRSF1 still showed nuclear localization when YAP was knocked down (Supplemental Fig. 7 A and B). These results suggested that YAP regulates the expression but not the subcellular localization of SRSF1.

Then, the possible regulatory effect of YAP on VEGF$_{165}$ expression and angiogenesis was further demonstrated. In comparison with negative control siRNA, si-RNA targeting YAP significantly decreased the mRNA level VEGF$_{165}$ (Fig. 3I). Secretion of VEGF$_{165}$ into the conditioned medium was also significantly decreased when YAP was knocked down by siRNA (Fig. 3J). The tube formation capacity of HUVECs was also suppressed under stimulation with conditioned medium from SK-N-SH cells with YAP repression (Fig. 3 K and L).

Taken together, the above in vitro results showed that YAP modulates the expression of SRSF1 at the transcriptional level, which contributes to VEGF$_{165}$ secretion and subsequent NB angiogenesis.

## YAP regulated SRSF1 through RUNX2

Since YAP modulated SRSF1 expression at the transcriptional level, we then demonstrated the mechanism underlying this regulatory process. Analysis of JASPAR, a database of potential transcription factor binding profiles, revealed that Runt-related factor 2 (RUNX2) has several potential binding sites in the promoter region of SRSF1 (Fig. 4A and B, Supplemental Table S5). In addition, multiple studies have shown that RUNX2 is an important mediator of mechanical cues initiated by the cellular microenvironment [29].

In SK-N-SH cells, RUNX2 protein expression was significantly decreased on the 30 kPa substrate compared with the 1 kPa, 8 kPa and plastic substrates, the same trend as the YAP and SRSF1 variations (Fig. 4C). ChIP was then used to investigate the binding of RNNX2 to the promoter region of SRSF1 in SK-N-SH cells, and the results revealed significant enrichment of RUNX2 in the SRSF1 promoter region (Fig. 4D).

Moreover, siRNA-mediated knockdown of RUNX2 in SK-N-SH cells (Supplemental Fig. 4C) resulted in a significant decrease in SRSF1 expression at both the mRNA and protein levels (Fig. 4E and F). These data suggested that in SK-N-SH cells, RUNX2 regulates SRSF1 expression by directly binding to the SRSF1 promoter.

Next, we sought to determine whether RUNX2 participates in the regulation of SRSF1 by YAP. Specific siRNA targeting YAP significantly repressed the expression of RUNX2, which indicated that YAP modulates the expression of RUNX2 (Fig. 4G). For YAP overexpression, the function of YAP-GFP construct was firstly confirmed by the mRNA expressions of downstream targets, including CTGF, ANKRD1 and CyR61. The results showed that the mRNA levels of these three molecules were increased in YAP overexpression group in comparison with the negative control (Supplemental Fig. 8). Overexpression of YAP increased the protein expression of SRSF1, while cotransfection of RUNX2 siRNA attenuated the increase in SRSF1 expression caused by YAP overexpression. Taken together, these data substantiated the hypothesis that the regulation of SRSF1 by YAP is dependent on RUNX2 in SK-N-SH cells.

## Implantation of nude mice with 3D gels confirmed that ECM stiffness regulates NB angiogenesis

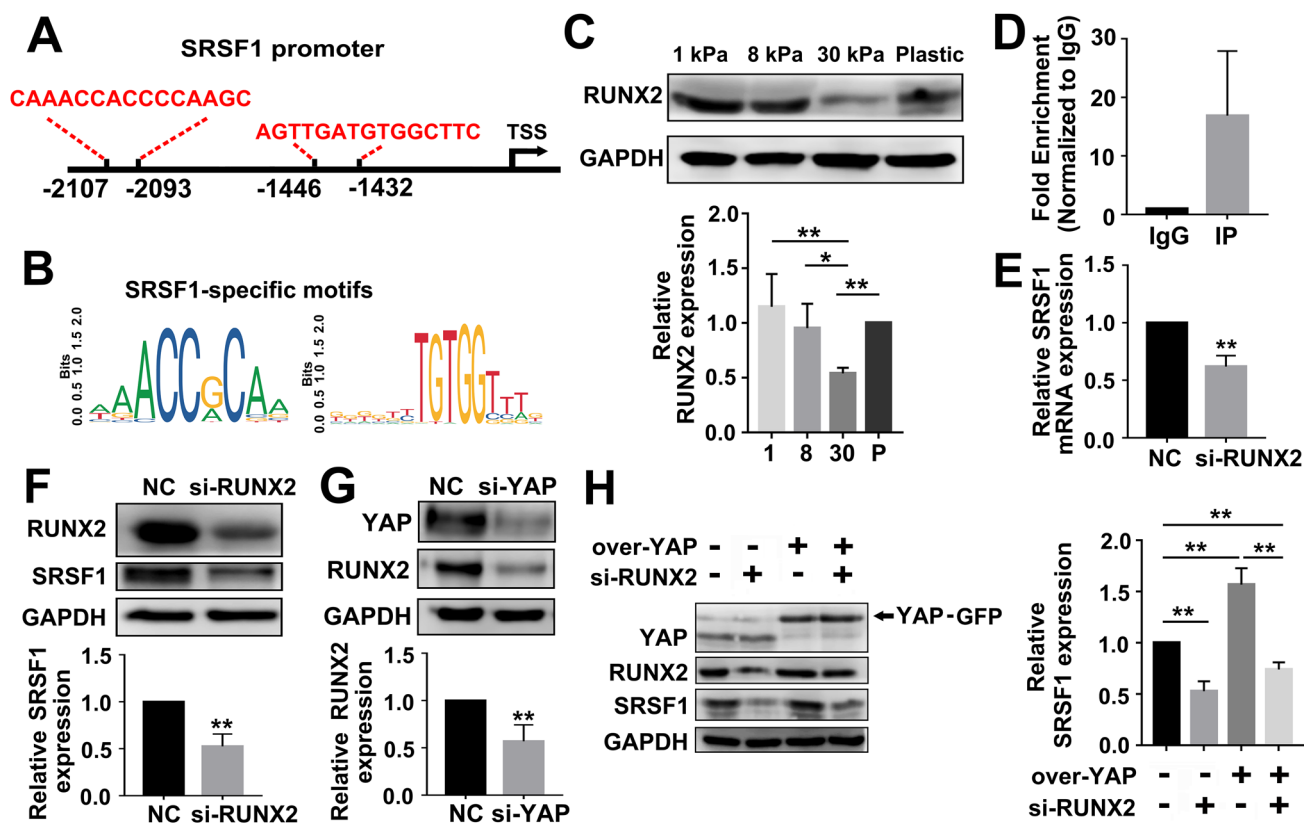To further identify whether ECM stiffness can regulate NB angiogenesis in vivo, we adopted a 3D culture system

**Fig. 4** YAP regulates SRSF1 through RUNX2. **A** The JASPAR database predicted the potential binding sites of RUNX2 at SRSF1 promoter region. **B** The specific motifs in the SRSF1 DNA segments immunoprecipitated with RUNX2. **C** The protein levels of RUNX2 in SK-N-SH cells seeded on 1 kPa, 8 kPa, 30 kPa and plastic substrates ($n=5$). **D** After immunoprecipitation with RUNX2 or IgG, qPCR detected the levels of SRSF1 promoter region ($n=3$). **E** The mRNA levels of SRSF1 after decreasing RUNX2 by si-RNA in SK-N-SH cells ($n=5$). **F** The protein levels of SRSF1 after decreasing RUNX2 by si-RNA in SK-N-SH cells ($n=5$). **G** The protein levels of RUNX2 after decreasing YAP by si-RNA in SK-N-SH cells ($n=5$). **H** Respective or co-transfection of YAP overexpression plasmid (YAP followed with GFP) and RUNX2 si-RNA were performed in SK-N-SH cells. The histogram result showed the relative protein level of SRSF1 ($n=5$). Values were shown as the mean ± SD, *$P<0.05$, **$P<0.01$ vs. the indicated groups or negative control (NC)

with different stiffnesses based on a transglutaminase-crosslinked gelatin gel (Col-Tgel) in nude mice. 3D gels of three different stiffnesses were individually mixed with SK-N-SH tumor cells and subcutaneously embedded on both sides of the abdomen in mice (Fig. 5A). The size and weight of Col-Tgels with different stiffness showed no obvious difference (Supplemental Fig. 9A and B). Furthermore, clear blood vessels appeared in the 1 kPa and 8 kPa stiffness Col-Tgels, but were not apparent in the 30 kPa 3D Col-Tgel (Fig. 5B and C, Supplemental Fig. 9A). The blood vessels in Col-Tgels with different stiffness were quantified with Angiotool software, which showed that blood vessels length in 1 kPa and 8 kPa 3D Col-Tgels was significantly increased compared with that in 30 kPa Col-Tgels (Supplemental Fig. 9C). By immunostaining of CD31, CD105 and vWF, vessel formation was easy to observe in the 1 kPa and 8 kPa 3D Col-Tgels but not in the 30 kPa 3D Col-Tgel (Fig. 5D, Supplemental Fig. 9D).

Immunostaining showed that SRSF1 was located in the nucleus in all three stiffness groups, while the intensity of SRSF1 in SK-N-SH cells was significantly decreased in the 30 kPa Col-Tgel compared with the 1 kPa and 8 kPa Col-Tgels (Fig. 5E and G). In addition, the nuclear distribution of YAP in SK-N-SH cells in the 30 kPa Col-Tgel was significantly decreased compared with that in the 1 kPa and 8 kPa Col-Tgels (Fig. 5F, H).

In this in vivo 3D Col-Tgel system, the 30 kPa stiffness showed a repressive effect on NB angiogenesis compared with the 1 kPa and 8 kPa stiffnesses. Furthermore, the expression of YAP, especially in the nucleus, was decreased under the 30 kPa condition. SRSF1 localization did not change with Col-Tgel stiffness, but its expression was decreased in the 30 kPa Col-Tgel. In summary, the variations observed in the in vivo 3D culture system were consistent with those in vitro.

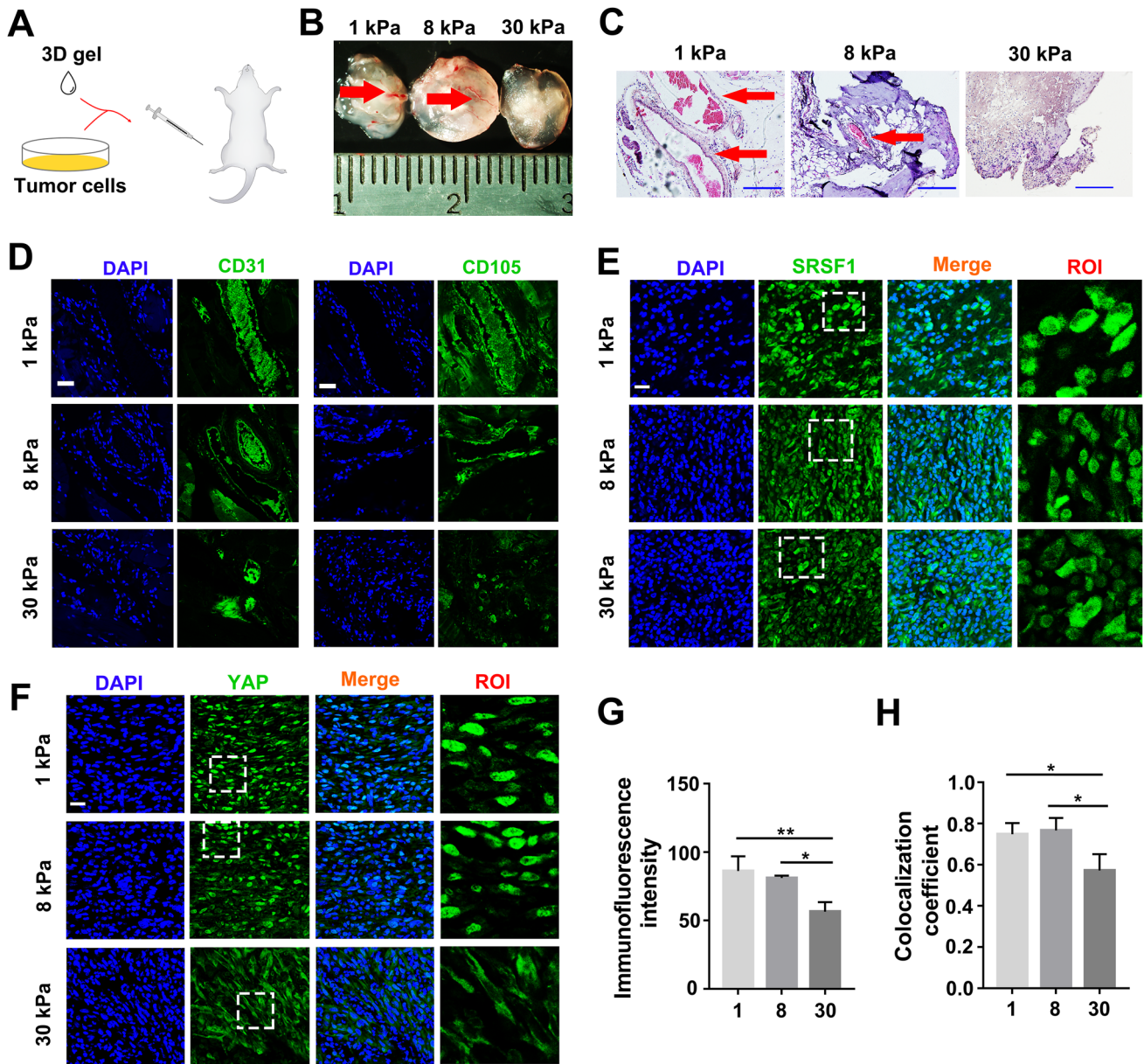Fig. 5 ECM stiffness regulates NB angiogenesis with xenograft tumor induction using Col-Tgel. **A** $1.0 \times 10^6$ SK-N-SH cells and 100 μL Col-Tgels with 1 kPa, 8 kPa and 30 kPa stiffness were mixed and, respectively, injected at the abdominal subcutaneous sites before gels curing. **B** The different stiffness Col-Tgels were excised after seven days and the blood vessel formation was detected (red arrows) ($n = 5$). **C** H&E staining of 1 kPa, 8 kPa and 30 kPa stiffness Col-Tgels with SK-N-SH cells. Red arrows showed the blood vessels (scale bar $= 200$ μm). **D** Immunostaining of CD31 and CD105, respectively, (green) exhibited the blood vessels formation capacity in different stiffness Col-Tgels (scale bar $= 40$ μm). **E** Immunostaining of SRSF1 (green) showed the expression and subcellular localization of SRSF1 in different stiffness Col-Tgels (scale bar $= 20$ μm). **F** Immunostaining of YAP (green) showed the expression and subcellular localization of YAP in different stiffness Col-Tgels (scale bar $= 20$ μm). **G** Immunofluorescence intensity of SRSF1 in 1 kPa, 8 kPa and 30 kPa 3D Col-Tgels ($n = 3$). **H** Colocalization coefficient of YAP with nucleus in 1 kPa, 8 kPa and 30 kPa 3D Col-Tgels ($n = 3$). Values were shown as the mean $\pm$ SD, $*P < 0.05$, $**P < 0.01$ vs. the indicated groups

## YAP was required for ECM stiffness-mediated NB angiogenesis

We further confirmed the role of YAP in NB angiogenesis both in vitro and in vivo. Since the above results revealed a repressive effect of the 30 kPa on YAP expression, we overexpressed YAP and evaluated the changes in NB angiogenesis.

YAP overexpression under the 30 kPa condition increased the secretion of $VEGF_{165}$ from SK-N-SH NB

cells compared with negative control cells (transfected with empty pcDNA-3.3 plasmid) on the 30 kPa substrate (Fig. 6A). The tube formation capacity of HUVECs was also increased by conditioned medium from YAP-overexpressing SK-N-SH cells cultured on the 30 kPa substrate (Fig. 6B and C).

In the 3D Col-Tgel culture system, 30 kPa hydrogels mixed with SK-N-SH cells overexpressing YAP were injected. When the 3D Col-Tgels were excised after 7 days, apparent blood vessels were observed in the YAP-overexpressing group compared with the negative control group (Fig. 6D and E). Immunostaining of vWF revealed that compared with that in the negative control group, blood vessel formation was markedly increased when YAP was overexpressed (Fig. 6F). Furthermore, immunostaining of SRSF1 showed that YAP overexpression also increased the SRSF1 fluorescence intensity in the 30 kPa Col-Tgel (Fig. 6G and H).

Taken together, the above results indicated that the repressive effect of the 30 kPa stiffness on NB angiogenesis was reversed by overexpression of YAP, and that the repression of SRSF1 through YAP may participate in this process.

## Discussion

The ECM, an important component of cell environment, is mainly composed of proteins and polysaccharides. Accumulating studies have shown that an imbalanced ECM remodeling during solid tumor progression causes variations in ECM stiffness and affects tumor cell functions. Han et al. demonstrated that the proliferation of breast cancer cells, as detected by immunostaining for Ki67, was higher on stiffer substrate than on softer substrate [30]. Andrew and colleagues showed that ECM stiffness regulates not only ovarian tumor cell migration but also cell morphology in a 2D culture system [31]. The stiffness of ECM could also regulate NB cell differentiation, proliferation and gene expression [32]. Our present study showed that ECM stiffness can modulate NB behaviors that are relevant to angiogenesis. TCGA database analysis revealed that the original sites of NB were distributed across a wide variety of tissues, and diverse mechanical microenvironments were possibly encountered in these tissues. Hence, we speculated that there was a unique regulatory mechanism underlying the regulation of NB angiogenesis by ECM stiffness.

Intriguingly, this relationship between ECM stiffness and angiogenic capabilities may involve complex mechanisms. For example, in different pathological status of tumors the
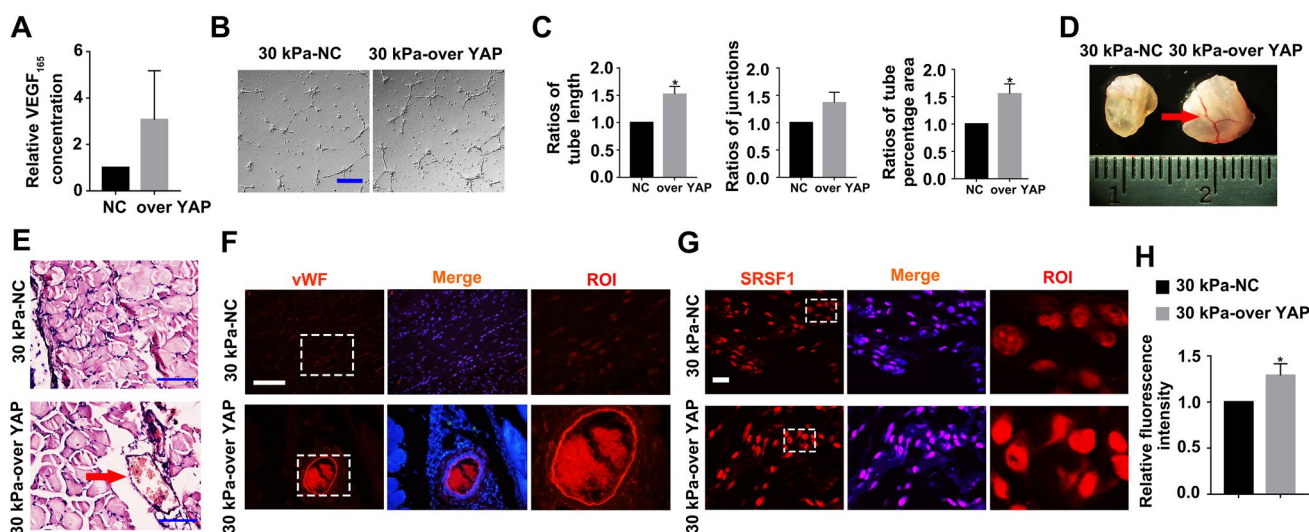


Fig. 6 YAP is required for ECM stiffness-mediated NB angiogenesis. A ELISA detected the $VEGF_{165}$ secretion from SK-N-SH cells with YAP overexpression on 30 kPa substrates ($n=5$). B The tube formation of HUVECs stimulated by conditioned medium from SK-N-SH cells with YAP overexpression on 30 kPa substrates (scale bar = 100 μm) ($n=3$). C The total tube length, number of junctions and tube percentage area were measured by Angiotool software. D The 30 kPa stiffness Col-Tgels with SK-N-SH cells overexpressing YAP were excised after 7 days and the blood vessel formation was exhibited (red arrows) ($n=3$). E H&E staining of 30 kPa stiffness Col-Tgels with SK-N-SH cells overexpressing YAP. Red arrows showed the blood vessels (scale bar = 100 μm). F Immunostaining of vWF (red) exhibited the blood vessels formation capacity in 30 kPa stiffness Col-Tgel with YAP overexpression (scale bar = 100 μm). G Immunostaining showed the expression and subcellular localization of SRSF1 (red) in 30 kPa stiffness Col-Tgel (scale bar = 40 μm). H Immunofluorescence intensity of SRSF1 in 30 kPa Col-Tgel with YAP overexpression ($n=3$). Values were shown as the mean±SD, *$P<0.05$, **$P<0.01$ vs. negative control (NC)

roles of stiffness variations in tumor angiogenesis are different [13]. Here we found a nonlinear relationship between ECM stiffness and NB angiogenesis. This nonlinear relationship had been also reported mesenchymal stem cells [33, 34]. Although the stiffnesses of our collected NB clinical samples were lower than 10 kPa, our in vitro studies suggested that a stiffness of 30 kPa repressed the expression and secretion of $VEGF_{165}$, an important regulator of angiogenesis, in NB cells. Cells of many established human NB cell lines have the capacity to differentiate when induced by different kinds of stimulation, and these cell lines have been used as models for studying and understanding central concepts of tumor cell differentiation [35]. One recent related discovery is the observation that NB cells can dedifferentiate and gain a stem cell-like phenotype during hypoxic conditions [36]. We observed that a 30 kPa stiffness-induced SK-N-SH cells to exhibit a larger spreading area and an increasingly branched, filopodia-rich morphology, which is similar to that of neurocytes (Supplemental Fig. 10). Whether NB cells tend to differentiate into neurocytes under a 30 kPa stiffness condition will be a very interesting question to answer and should be addressed in the future. Our present results suggested that a 30 kPa stiffness inhibits the secretion of $VEGF_{165}$ and attenuates NB angiogenesis. This finding may suggest that NB prognosis is correlated with tissues stiffness. Furthermore, several previous studies have showed that modulating ECM stiffness of tumor tissues could improve drug-sensitivity [37], repress tumor angiogenesis and raise survival rate in clinical practice [13]. These studies indicated that targeting ECM stiffness may be a therapeutic approach for NB with clinical potential.

VEGF-A is a well-characterized factor that facilitates vascular formation [38]. VEGF-A has different isoforms and $VEGF_{165}$ is the most potent initiator of angiogenesis. The role of $VEGF_{165}$ in angiogenesis was reported in previous researches [39]. $VEGF_{165}$ is generated by alternative splicing, which is the main regulator of the increased protein-to-gene ratio and is involved in the formation of diverse mature mRNAs from a single pre-mRNA [40]. The human *Vegf-a* gene consists of eight exons and seven introns. Exons 1–5 are constitutive exons and are therefore present in all VEGF-A isoforms. Alternative splicing of VEGF-A pre-mRNA selectively removes intronic regions and joins specific combinations of exons to generate distinct VEGF-A isoforms [41]. SR proteins have been characterized as key splicing factors during the alternative splicing of VEGF-A [42]. Our present study revealed that SRSF1 participates in the generation of $VEGF_{165}$ isoform in NB cells responsive to different stiffnesses. SRSF1 is a typical alternative splicing factor in the SR protein family that is tightly linked to VEGF-A alternative splicing [43]. Abnormal expression of SRSF1 is related to multiple diseases, especially tumors [44]. From analysis of the Gene Expression Profiling Interactive Analysis

(GEPIA) database, we found that SRSF1 expression positively correlates with poor prognosis and overall survival in carcinoma patients (Supplemental Fig. 11A). Upregulation of SRSF1 was observed in glioma clinical samples [45]. Furthermore, increased levels of SRSF1-induced upregulation of target oncogenes [46]. In our studies, we confirmed that compared with 1 kPa and 8 kPa stiffness, 30 kPa stiffness decreases SRSF1 expression and revealed that YAP is an initial upstream regulator of SRSF1.

YAP is a core component of the Hippo pathway [47], which is evolutionarily conserved and has multiple biological functions in the development, homeostasis, and regeneration of tissues and organs [48]. YAP is a transcriptional coactivator that shuttles between the nucleus and the cytoplasm. Activated (unphosphorylated statue) YAP is located in the nucleus and recognizes cognate cis-regulatory elements by interacting with other transcription factors, particularly TEA domain (TEAD) family members. In contrast, phosphorylation of YAP leads to its cytoplasmic sequestration, which inhibits its activity [49]. Studies have shown that expression of YAP is essential for tumor initiation, progression and metastasis in many kinds of cancers. Based on analysis of the GEPIA database, we found that YAP expression positively correlates with poor prognosis and overall survival in carcinoma patients (Supplemental Fig. 11B). YAP is overexpressed in pancreatic clinical samples [50]. Furthermore, elevated YAP expression in human glioma cells promotes tumorigenesis in tumorigenesis models [51]. When YAP was knocked down in the human LAC cell line A549, tumor formation was impaired after injection into nude mice [52]. In addition, enhanced YAP expression was found to lead to drug resistance, which is an intractable problem in antitumor therapy for lung carcinoma [53].

Except for the expression level, the activation of YAP has also been widely proven to be involved in tumor progression. Accumulation of YAP in the nucleus was induced by transgenic expression of ILK which accelerated the growth of mammary gland tumors in mice [54]. Furthermore, activation of YAP induced the transcription of associated genes, which results in a stem-like cell population in lung cancer cells [55]. In addition, YAP plays a central role in mechanotransduction to regulate cellular functions [28]. Several studies showed that YAP is activated in the stiffer ECM. For example, a soft ECM induces epidermal stem cell differentiation by inhibiting YAP/TAZ [56]. In our studies, we found that the nuclear accumulation of YAP was decreased under the 30 kPa condition. The effect of ECM stiffness on YAP is quite complicated and interesting. For example, malignancy grade of tumors plays a role in the localization of YAP regulated by ECM stiffness. Liu and colleagues showed that in breast cancer cells, the nuclear localization of YAP is significantly higher in 38 kPa (malignant tumor) compared with 10 kPa
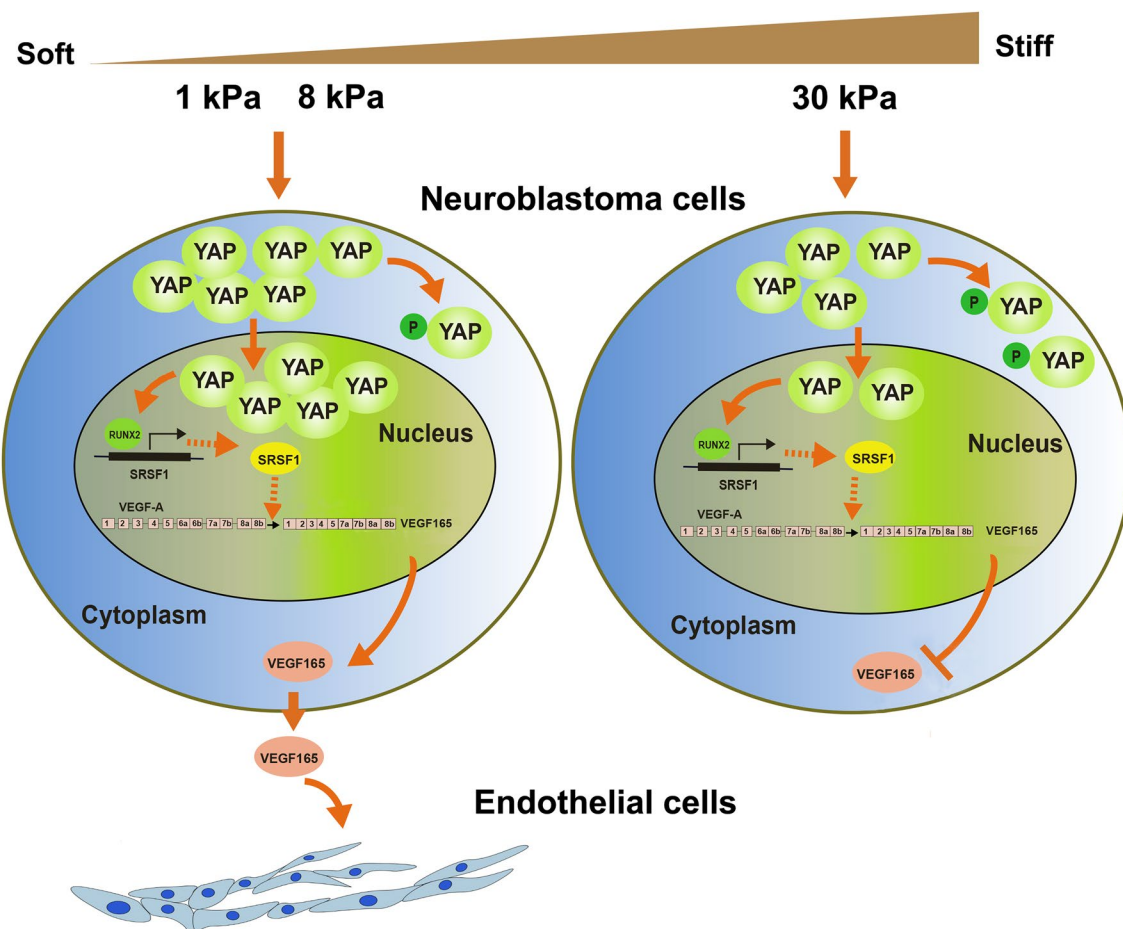
**Fig. 7** Schematic drawing of the mechanisms of NB angiogenesis induced by ECM stiffness

(fibrous tumor) and 57 kPa (tissue stiffness during bone metastasis), which suggested that the nonlinear relationship of ECM stiffness and YAP nuclear expression depend on the malignancy grade in breast cancer [57]. Additionally, different cellular state may also influence subcellular localization of YAP. For example, YAP nuclear expression is increased by stiffer ECM in children derived MSCs. Whereas in adults derived MSCs, YAP shows cytoplasmic expression with the increase of ECM stiffness due to the loss of mechanically sensitivity [58]. These studies suggested the role of stiffness in YAP expression and location is quite complex with tissue specificity, different pathological situation, and et al.

Taken together, our data showed that ECM stiffness influences NB angiogenesis by regulating the communication between tumor cells and ECs (Fig. 7). Moreover, we confirmed that the YAP-RUNX2-SRSF1 axis is mechanoresponsive to ECM stiffness and modulates the secretion of VEGF$_{165}$. These observations supported further investigations of the role of microenvironmental mechanical signals in NB angiogenesis, and suggested that modulating

ECM stiffness and potential mechanoresponsive molecules may have a role in NB therapy.

## Declarations

**Conflict of interest** The authors declare that they have no conflict of interest.

## References

1. Ambros PF, Ambros IM, Brodeur GM et al (2009) International consensus for neuroblastoma molecular diagnostics: report from the International Neuroblastoma Risk Group (INRG) Biology Committee. Br J Cancer 100(9):1471–1482

2. Cox TR, Erler JT (2011) Remodeling and homeostasis of the extracellular matrix: implications for fibrotic diseases and cancer. Dis Model Mech 4(2):165–178

3. Paszek MJ, Zahir N, Johnson KR et al (2005) Tensional homeostasis and the malignant phenotype. Cancer Cell 8(3):241–254

4. Engler AJ, Sen S, Sweeney HL et al (2006) Matrix elasticity directs stem cell lineage specification. Cell 126(4):677–689

5. Handorf AM, Zhou YX, Halanski MA et al (2015) Tissue stiffness dictates development, homeostasis, and disease progression. Organogenesis 11(1):1–15

6. Meng ZP, Qiu YJ, Lin KC et al (2018) RAP2 mediates mechanoresponses of the Hippo pathway. Nature 560(7720):655–660

7. Jeong J, Keum S, Kim D et al (2018) Spindle pole body component 25 homolog expressed by ECM stiffening is required for lung cancer cell proliferation. Biochem Biophys Res Commun 500(4):937–943

8. Pathak A, Kumar S (2012) Independent regulation of tumor cell migration by matrix stiffness and confinement. Proc Natl Acad Sci USA 109(26):10334–10339

9. Peng YT, Chen ZY, Chen Y et al (2019) ROCK isoforms differentially modulate cancer cell motility by mechanosensing the substrate stiffness. Acta Biomater 88:86–101

10. Lam WA, Cao LZ, Umesh V et al (2010) Extracellular matrix rigidity modulates neuroblastoma cell differentiation and N-myc expression. Mol Cancer 9:35

11. Bordeleaua F, Masona BN, Lollis EM et al (2016) Matrix stiffening promotes a tumor vasculature phenotype. Proc Natl Acad Sci USA 114(3):492–497

12. López MR, Trinh AL, Sobrino A et al (2017) Recapitulating the human tumor microenvironment: colon tumor-derived extracellular matrix promotes angiogenesis and tumor cell growth. Biomaterials 116:118–129

13. Shen Y, Wang XH, Lu JY et al (2020) Reduction of liver metastasis stiffness improves response to bevacizumab in metastatic colorectal cancer. Cancer Cell 37(6):800–817

14. Shoval H, Bluman AK, Karniely YB et al (2017) Tumor cells and their crosstalk with endothelial cells in 3D spheroids. Sci Rep 7(1):10428

15. Sarkar S, Peng CC, Tung YC (2020) Comparison of VEGF-A secretion from tumor cells under cellular stresses in conventional monolayer culture and microfluidic threedimensional spheroid models. PLoS ONE 15(11):e0240833

16. Jakovljević G, Жulić S, Stepan J et al (2009) Vascular endothelial growth factor in children with neuroblastoma: a retrospective analysis. J Exp Clin Cancer Res 28(1):143

17. Chanthery YH, Gustafson WH, Itsara M et al (2012) Paracrine signaling through MYCN enhances tumor-vascular interactions in neuroblastoma. Sci Transl Med 4(115):115ra3

18. Pasquale MD, Castellano A, Sio L et al (2011) Bevacizumab in pediatric patients: how safe is it? Anticancer Res 31(11):3953–3957

19. Geretti E, Shimizu A, Klagsbrun M (2008) Neuropilin structure governs VEGF and semaphorin binding and regulates angiogenesis. Angiogenesis 11(1):31–39

20. Mattei G, Gruca G, Rijnveld N et al (2015) The nano-epsilon dot method for strain rate viscoelastic characterisation of soft biomaterials by spherical nano-indentation. J Mech Behav Biomed Mater 50:150–159

21. Poursaleh A, Esfandiari G, Beigee FS et al (2019) Isolation of intimal endothelial cells from the human thoracic aorta: study protocol. Med J Islam Repub Iran 33:51

22. Tse JR, Engler AJ (2010) Preparation of Hydrogel substrates with tunable mechanical properties. Curr Protoc Cell Biol Chap 10: Unit. 10.16

23. Artola AE, Andreu I, Beedle AEM et al (2017) Force tiggers YAP nuclear entry by regulating transport across nuclear pores. Cell 171(6):1397–1410

24. Matsuzaki S, Canis M, Pouly JL et al (2015) Soft matrices inhibit cell proliferation and inactivate the fibrotic phenotype of deep endometriotic stromal cells in vitro. Hum Reprod 31(3):541–553

25. James GC, Melissa G, Gopinath D et al (2015) The carboxyl terminus of VEGF-A is a potential target for anti-angiogenic therapy. Angiogenesis 18(1):23–30

26. WagnerKD, Maï ME, Michael L et al (2019) Altered VEGF splicing isoform balance in tumor endothelium involves activation of splicing factors Srpk1 and Srsf1 by the Wilms' tumor suppressor Wt1. Cells 8(1):41

27. Dupont S, Morsut L, Aragona M et al (2011) Role of YAP/TAZ in mechanotransduction. Nature 474(7350):179–183

28. Dobrokhotov O, Samsonov M, Sokabe M et al (2018) Mechanoregulation and pathology of YAP/TAZ via Hippo and non-Hippo mechanisms. Clin Transl Med 7(1):23

29. Kruik AM, Villasante A, Yaeger K et al (2018) Biomechanical regulation of drug sensitivity in an engineered model of human tumor. Biomaterials 150:150–161

30. Han SY, Pang MF, Nelson CM et al (2018) Substratum stiffness tunes proliferation downstream of Wnt3a in part by regulating integrin-linked kinase and frizzled-1. J Cell Sci 131(8):jcs210476

31. McKenzie AJ, Hicks SR, Svec KV et al (2018) The mechanical microenvironment regulates ovarian cancer cell morphology, migration, and spheroid disaggregation. Sci Rep 8(1):7228

32. Tadeo I, Berbegall AP, Castel V et al (2016) Extracellular matrix composition defines an ultra-high-risk group of neuroblastoma within the high-risk patient cohort. Br J Cancer 115(4):480–489

33. Abdeen AA, Weiss JB, Lee J et al (2014) Matrix composition and mechanics direct proangiogenic signaling from mesenchymal stem cells. Tissue Eng Part A 20(19–20):2737–2745

34. Bandaru P, Cefaloni G, Vajhadin F et al (2020) Mechanical cues regulating proangiogenic potential of human mesenchymal stem cells through YAP-mediated. Mechanosens Small 16(25):e2001837

35. Mao L, Ding J, Zha YH (2011) HOXC9 links cell cycle exit and neuronal differentiation and is a prognostic marker in neuroblastoma. Cancer Res 71(12):4314–4324

36. Jogi A, Øraa I, Nilsson H et al (2003) Hypoxia-induced dedifferentiation in neuroblastoma cells. Cancer Lett 197(1–2):145–150

37. Vennin C, Chin VT, Warren SC et al (2017) Transient tissue priming via ROCK inhibition uncouples pancreatic cancer progression, sensitivity to chemotherapy, and metastasis. Sci Transl Med 9(384):eaai8504

38. Joseph WF, Aaron BB, Vipul CC et al (2011) Stromal endothelial cells directly influence cancer progression. Sci Transl Med 3(66):66ra5

39. Duinen VV, Zhu D, Remakers C et al (2019) Perfused 3D angiogenic sprouting in a high-throughput in vitro platform. Angiogenesis 22(1):157–165

40. Michael RL, Steven JH, David OB (2007) Alternative splicing in angiogenesis: the vascular endothelial growth factor paradigm. Cancer Lett 249(2):133–142

41. Arconde´guy T, Lacazette E, Millevoi S (2013) VEGF-A mRNA processing, stability and translation: a paradigm for intricate regulation of gene expression at the post-transcriptional level. Nucleic Acids Res 41(17):7997–8010

42. Maria PP (2012) The role of VEGF165b in pathophysiology. Cell Adhes Migr 6(6):1–8

43. Dawid GN, Elianna A, Emma SR et al (2010) Regulation of vascular endothelial growth factor (VEGF) splicing from pro-angiogenic to anti-angiogenic isoforms. J Biol Chem 285(8):5532–5540

44. Shipra D, Adrian RK (2014) Emerging functions of SRSF1, splicing factor and oncoprotein, in RNA metabolism and cancer. Mol Cancer Res 12(9):1195–1204

45. Zhou XX, Wang R, Li XB et al (2019) Splicing factor SRSF1 promotes gliomagenesis via oncogenic splice-switching of MYO1B. J Clin Invest 129(2):676–693

46. Chen LL, Luo C, Shen L et al (2017) SRSF1 prevents DNA damage and promotes tumorigenesis through regulation of DBF4B PremRNA splicing. Cell Rep 21(12):3406–3413

47. Piccolo S, Dupont S, Cordenonsi M (2014) The biology of YAP/TAZ: hippo signaling and beyond. Physiol Rev 94(4):1287–1312

48. Iván MM, Georg H (2019) Hippo-YAP/TAZ signalling in organ regeneration and regenerative medicine. Nat Rev Mol Cell Biol 20(4):211–226

49. John ML, Patrick S, Liu H et al (2012) The Hippo pathway target, YAP, promotes metastasis through its TEAD-interaction domain. Proc Natl Acad Sci USA 109(37):E2441–E2450

50. Jiang ZD, Zhou CC, Cheng L et al (2018) Inhibiting YAP expression suppresses pancreatic cancer progression by disrupting tumor-stromal interactions. J Exp Clin Cancer Res 37(1):69

51. Liu ZJ, Yee PP, Wei YJ et al (2019) Differential YAP expression in glioma cells induces cell competition and promotes tumorigenesis. J Cell Sci 132(5):jcs225714

52. Lau AN, Curtis SJ, Fillmore CM et al (2014) Tumor-propagating cells and Yap/Taz activity contribute to lung tumor progression and metastasis. EMBO J 33(5):468–481

53. Lee TF, Tseng YC, Nguyen PA et al (2017) Enhanced YAP expression leads to EGFR TKI resistance in lung adenocarcinomas. Sci Rep 8(1):271

54. Serrano I, McDonald PC, Lock F (2013) Inactivation of the Hippo tumour suppressor pathway by integrin-linked kinase. Nat Commun 4:2976

55. Pankova D, Jiang YY, Chatzifrangkeskou M et al (2019) RASSF1A controls tissue stiffness and cancer stem-like cells in lung adenocarcinoma. EMBO J 38(13):e100532

56. Totaro A, Castellan M, Battilana G et al (2017) YAP/TAZ link cell mechanics to Notch signalling to control epidermal stem cell fate. Nat Commun 8:15206

57. Qin X, Lv XY, Li P et al (2020) Matrix stiffness modulates ILK-mediated YAP activation to control the drug resistance of breast cancer cells. Biochim Biophys Acta Mol Basis Dis 1866(3):165625

58. Barreto S, Vazquez AG, Cameron AR et al (2017) Identification of the mechanisms by which age alters the mechanosensitivity of mesenchymal stromal cells on substrates of differing stiffness: implications for osteogenesis and angiogenesis. Acta Biomater 53:59–69